



Detection of weak transient signals based on wavelet packet transform and manifold learning for rolling element bearing fault diagnosis

Yi Wang ^a, Guanghua Xu ^{a,b,*¹}, Lin Liang ^a, Kuosheng Jiang ^a

^a School of Mechanical Engineering, Xi'an Jiaotong University, Xi'an 710049, PR China

^b State Key Laboratory for Manufacturing Systems Engineering, Xi'an Jiaotong University, Xi'an 710049, PR China



ARTICLE INFO

Article history:

Received 28 November 2013

Received in revised form

1 May 2014

Accepted 2 September 2014

Available online 14 October 2014

Keywords:

Rolling element bearing
Wavelet packet transform
Manifold learning
Permutation entropy
Fault diagnosis

ABSTRACT

The kurtogram-based methods have been proved powerful and practical to detect and characterize transient components in a signal. The basic idea of the kurtogram-based methods is to use the kurtosis as a measure to discover the presence of transient impulse components and to indicate the frequency band where these occur. However, the performance of the kurtogram-based methods is poor due to the low signal-to-noise ratio. As the weak transient signal with a wide spread frequency band can be easily masked by noise. Besides, selecting signal just in one frequency band will leave out some transient features. Aiming at these shortcomings, different frequency bands signal fusion is adopted in this paper. Considering that manifold learning aims at discovering the nonlinear intrinsic structure which embedded in high dimensional data, this paper proposes a waveform feature manifold (WFM) method to extract the weak signature from waveform feature space which obtained by binary wavelet packet transform. Minimum permutation entropy is used to select the optimal parameter in a manifold learning algorithm. A simulated bearing fault signal and two real bearing fault signals are used to validate the improved performance of the proposed method through the comparison with the kurtogram-based methods. The results show that the proposed method outperforms the kurtogram-based methods and is effective in weak signature extraction.

© 2014 Elsevier Ltd. All rights reserved.

1. Introduction

Rolling element bearings are widely used in rotating machinery, faults occurring in bearings may lead to fatal breakdowns in rotating machinery and such failure can be catastrophic, resulting in costly downtime. Therefore, it is significant to accurately diagnose the existence of faults at an early stage. Vibration signals collected from bearings contain rich information on machine health conditions [1]. Hence, it is possible to obtain vital characteristic information from vibration signals through the use of advanced signal processing techniques due to their intrinsic advantage of revealing bearing failure [2].

The theoretical background of bearing failure mechanism has been covered quite comprehensively during the past decades. The transients or transient signals are generally referred to as the signal components composed of exponentially

* Corresponding author at: School of Mechanical Engineering, Xi'an Jiaotong University, Xi'an 710049, PR China. Tel.: +86 29 8266 4257.

E-mail address: xugh@mail.xjtu.edu.cn (G. Xu).

¹ Tel./fax: +86 29 8339 5054.

decaying ringing that lasts a short period of time and spans within a wide frequency range [3,4]. The signature of a defected bearing consists of transients or transient signals that occur approximate periodically at a characteristic frequency and the duration between two adjacent impulses has a slight randomness [5]. Fault diagnosis is achieved by detecting the weak transient signals and alerting maintenance personnel before the fault develops into a catastrophic failure.

As for the vibration signal of rolling element bearing, signal modulation effect and noise are two major barriers in incipient defect detection for bearing fault diagnosis [6]. In order to overcome the barrier of modulation, Randall [7] proposed a Fast Fourier Transform (FFT)-based Hilbert transform. Though FFT-based Hilbert transform offers an effective technique for signal demodulation, this method failed to address how to enhance the weak transients from a noisy signal, especially in early stage defects detection for bearing failure diagnosis.

To enhance the signal-to-noise ratio of the original signal, a signal representation method is first needed for the identification of transient feature and background noise. For transient feature representation and identification, the time-frequency representation (TFR) is the most frequently used method, through which the transient feature can be represented in time-frequency space [8]. The wavelet transform (WT) is actually a kind of TFR method, as the scale of the WT corresponds to the frequency [9]. The wide applications of WT are based on its distinct features such as the freedom of mother wavelet selection and the avoidance of cross items in traditional TFRs (e.g., Wigner–Ville distribution, Pseudo-Wigner–Ville). Though WT has some distinct features compared with the traditional TFR methods, WT cannot effectively split the high frequency band containing rich fault modulation information [10]. The way of overcoming this difficulty is to extend WT to wavelet packet transform (WPT). As one of the famous TFR techniques, WPT has the well-known properties of being orthogonal, complete, and local. Based on the above-mentioned distinct features, WPT can be used as an excellent signal representation method to enhance the weak transients from a noisy signal.

In recent years, several WPT-based optimal frequency-band selection methods for transient signal extraction have been proposed. Aiming at the shortcomings of the original kurtogram method [11], Lei et al. [1] proposed an improved kurtogram method to overcome the shortcomings by replacing the filter of the original kurtogram with WPT filter. Wang et al. [12] proposed an enhanced kurtogram method, the major innovation of which is that kurtosis values are calculated based on the power spectrum of the envelope of the signals extracted from the wavelet packet nodes at different WPT levels. Some other optimal filter band selection based transient signal extracting methods have also been proposed, such as protrogram [13], sparsogram [14] and adaptive spectral kurtosis [15]. The basic idea of the optimal filter band selection based methods is to exploit the possibility of using a metrics (such as kurtosis, sparsity, etc.) as a measure to discover the presence of transient impulse components and to indicate the frequency band these occur. Considering the fact that transient signals span within a wide frequency range, only selecting the reconstructed signal in one frequency band may leave out some important information. Besides, at the early stage of bearing defect development, the weak transient signal of a defective bearing with a wide spread frequency band can be easily masked by noise in each frequency band [16]. By the optimal frequency band selection methods, only the noises outside the selected frequency band are removed from the original signal, while those inside the selected frequency band cannot be wiped off effectively. As a result, the performances of those methods are poor in the presence of low signal-to-noise ratio.

Recently, manifold learning has emerged in nonlinear feature extraction, due to its capability in effectively identifying low-dimensional nonlinear intrinsic structure embedded in high-dimensional data. The technique can be realized through several algorithms including locally linear embedding (LLE) [17], isometric feature mapping (IsoMap) [18], local tangent space alignment (LTSA) [19], and Laplacian eigenmaps (LE) [20], etc. Many studies have been conducted by applying manifold learning to the machinery fault diagnosis [21–32]. In recent years, the application of manifold learning in mechanical fault diagnosis can be divided into two categories. On one hand, manifold learning is used to extract non-linear features for fault classification [21–28], on the other hand, this technique is applied to extract the transient signals from the noise contaminated signal [29–32]. The above mentioned studies have demonstrated that manifold learning is effective to extract the intrinsic manifold features related to non-linear dynamics of the mechanical system.

In this paper, the reconstructed signal in each time-frequency subspace is considered as waveform feature (WF). The binary WPT separates the signal waveform information into different time-frequency subspaces layer by layer, forming a kind of high-dimensional WF space. In other words, WF space is a fusion of different frequency band signals. Consider the merits of WF space in signal representation and the manifold learning in nonlinear intrinsic structure extraction, a novel waveform feature manifold (WFM) technique is proposed. Aiming at the shortcomings of the optimal filter band selection methods, the WFM technique intends to mine the nonlinear WF structure by manifold learning to obtain transient signal feature for bearing fault diagnosis. Minimal permutation entropy is used as a criterion to optimize the selection of the number of neighbourhoods in the manifold learning algorithm. In order to overcome the barrier of modulation, the envelope analysis is used for further demodulation of the extracted transient signal. The frequency signatures of the envelope spectrum are used to diagnose the type of bearing fault by identifying its characteristic frequency. As typical optimal filter band selection methods, the original kurtogram, the improved kurtogram and the enhanced kurtogram are used in this paper for comparison study, and to demonstrate the improved performance of the proposed WFM method.

The outline of this paper is as follows. Section 2 first reviews the theory of WPT and presents the algorithm to construct the waveform feature space from the binary WPT tree, then the main steps of manifold learning is introduced and a minimum permutation criterion is demonstrated, and finally, the algorithm of the proposed method is presented. And the

proposed method is verified by a simulated signal in [Section 3](#). In [Section 4](#), the proposed method is experimentally validated by two experimental cases of bearing signals. Finally, conclusions are drawn in [Section 5](#).

2. WFM for transient signal extraction

2.1. WPT based waveform feature space construction

Wavelet transform (WT) has perfect local properties in both time and frequency spaces, and can be used as an effective method to preserve signal characteristics. However, WT does not split the high frequency bands where the modulation information of machine fault always exists. A better representation of signal is extending WT to wavelet packet transform (WPT). WPT further decompose the high-frequency bands and the frequency resolution may be enhanced. A signal can be decomposed into a set of wavelet packet nodes with the form of a full binary tree by the WPT. Let $U_{0,0}$ be a vector space of R^n , corresponding to the node 0 of the parent tree. Then at each level the vector space is split into two mutually orthogonal subspaces given by the following equation:

$$U_{j,k} = U_{j+1,2k} \oplus U_{j+1,2k+1} \quad (1)$$

where j represents the level of the tree, and $k(k=0, \dots, 2^j - 1)$ indicates the node index in level j . The split is repeated until the maximum decomposition level J , producing 2^J mutually orthogonal subspaces.

The principle of WPT can be mathematically described as follows. First, the WP function $W_{j,k}^n(t)$ can be mathematically expressed as below [24]:

$$W_{j,k}^n(t) = 2^{j/2} W^n(2^j t - k) \quad (2)$$

where the integers j and k are the scale and translation parameters, respectively; $n = 0, 1, \dots$ is the oscillation parameter. The first two wavelet packet functions with $j = k = 0$ are the scaling function $\Phi(t)$ and mother wavelet function $\Psi(t)$ as below:

$$W_{0,0}^0(t) = \Phi(t) \quad (3)$$

$$W_{0,0}^1(t) = \Psi(t) \quad (4)$$

The remaining WP functions for $n = 2, 3, \dots$ are defined through the following recursive relationships:

$$W^{2n}(t) = \sqrt{2} \sum_k h(k) W_{1,k}^n(2t - k) \quad (5)$$

$$W^{2n+1}(t) = \sqrt{2} \sum_k g(k) W_{1,k}^n(2t - k) \quad (6)$$

where $h(k) = 1/\sqrt{2} \langle \varphi(t), \varphi(2t - k) \rangle$ and $g(k) = 1/\sqrt{2} \langle \psi(t), \psi(2t - k) \rangle$ are the filter coefficients of low-pass and high-pass filters respectively, and they are orthogonal with the relationship $g(k) = (-1)^k h(1-k)$. Here, $\langle \cdot, \cdot \rangle$ represents the inner product operator. The wavelet packet coefficients $S_{j,k}^n$ are obtained by the inner product between the signal $x(t)$ and the wavelet packet functions $W_{j,k}^n$, as below:

$$S_{j,k}^n = \langle x, W_{j,k}^n \rangle = \int_{-\infty}^{\infty} x(t) W_{j,k}^n(t) dt \quad (7)$$

As a result, at the j th level, the signal $x(t)$ is decomposed into 2^j packets with the order $n = 1, 2, \dots, 2^j$. In the binary tree structure, the nodes are indexed by (j, n) . According to each scale parameter j , the tree-structure of the WPT consists of multiple nodes with equal bandwidth. After the reconstruction of coefficients at each node layer by layer in the tree-structure, we get a waveform feature space.

Mathematically, for a discrete signal $x(t)$ with $N(N = 2^{n_0})$ points, the reconstructed signal of wavelet coefficients in node (j, n) can be denoted by $\{R_j^n(k), k = 1, 2, \dots, 2^{n_0}\}$. If we assume the WP node (j, n) is a container with the area of 2^{n_0} , so R_j^n is used to represent the waveform feature distributed in the container. The waveform feature (WF) matrix for the (j, n) th level can be written as below:

$$WF_j = \left\{ \begin{array}{l} x(t), j = 0 \\ \underbrace{[R_j^1]_{2^{n_0} \times 1} \cdots [R_j^n]_{2^{n_0} \times 1} \cdots [R_j^{2^j}]_{2^{n_0} \times 1}}_{n = 1, 2, \dots, 2^j} \end{array} \right\} \in R^{2^{n_0} \times 2^j}, j \in (1, J) \quad (8)$$

Put WF_j from level 0 to J together, and then the WF can be written as follows:

$$WF = \left[\underbrace{[WF_0]_{2^{n_0} \times 2^0} \cdots [WF_n]_{2^{n_0} \times 2^n} \cdots [WF_J]_{2^{n_0} \times 2^J}}_{n = 1, 2, \dots, J} \right]^T \in R^{D \times 2^{n_0}} \quad (9)$$

where $D = 2^0 + 2^1 + \dots + 2^J$, i.e. the dimension of the waveform feature matrix.

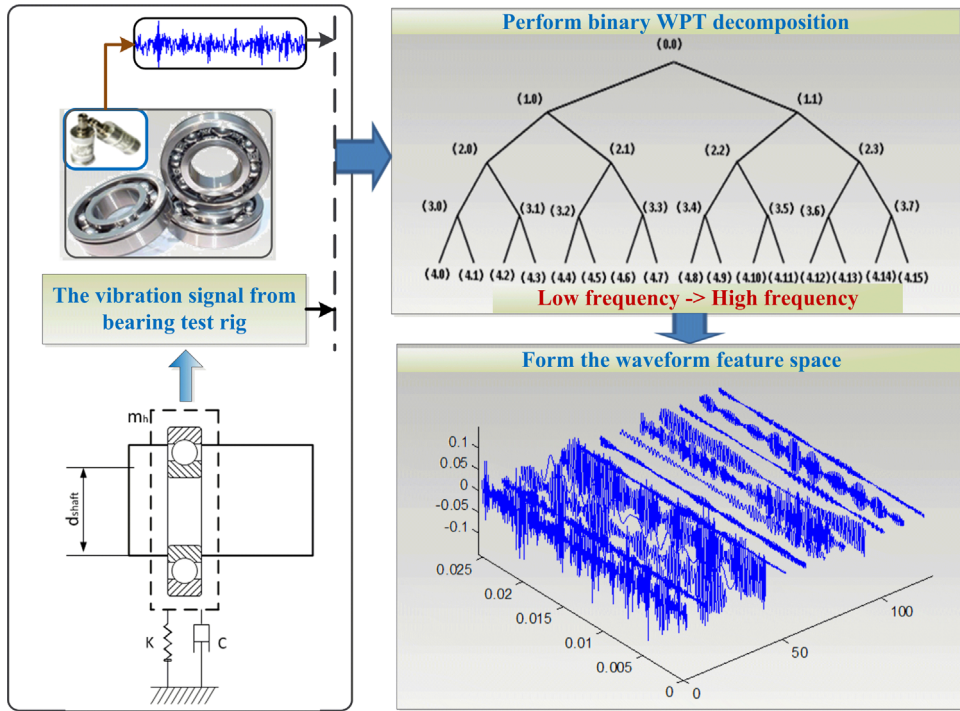


Fig. 1. WPT based waveform feature space construction.

The process of achieving the WF matrix is shown in Fig. 1. The WF matrix is a fusion of different frequency bands signals, and it reveals the waveform feature of the analysed signal in different time–frequency subspaces. Considering the fact that weak transient signal span within a wide frequency range, some important information may leave out after selecting the reconstructed signal in one frequency band from the WPT tree. Besides, the weak transient signal feature in each frequency band can be easily masked by noise. As a result, by optimal frequency band selection, only the noises outside the selected frequency band are removed from the original signal, while those inside the selected frequency band cannot be wiped off effectively. In this study, the weak transient signal is regarded as a nonlinear waveform feature embedded in the high-dimensional WF matrix, which motivates our following study on nonlinear waveform feature extraction.

2.2. WF manifold learning

Manifold learning aims at discovering the nonlinear structure embedded in the high dimensional data. Several studies have been conducted by applying manifold learning to the machinery fault diagnosis [21–32]. They have demonstrated that the manifold learning is effective to extract the intrinsic manifold features related to nonlinear dynamics of mechanical systems. Thus it is hoped to capture the weak transient feature embedded in the waveform feature matrix by manifold learning technique. The technique can be realized through several algorithms, such as LLE [17], IsoMap [18], LTSA [19], and LE [20], etc. The LTSA technique, due to its robustness to parameters and advantages of principal manifold reconstruction [19], is frequently used in mechanical signal processing [30–32]. Considering LTSA is effective to extract the intrinsic manifold features related to non-linear dynamics of mechanical systems. Therefore LTSA technique is also employed for WFM learning. The following gives a succinct description of the algorithm for WFM learning.

Given the data set $X = [z_1, z_2, \dots, z_N]$ constructed in Eq. (9), with $z_i \in R^D$ as a point in the D dimensional space. The data points are assumed lie on or near a nonlinear manifold with an intrinsic dimensionality $d < D$ (typically $d \leq D$). The LTSA is used to find a low-dimensional embedding of X by mapping the D -dimensional data into an embedded space R^d . The algorithm of LTSA is shown in Fig. 2, and the main steps of LTSA are as follows:

- (1) *Extracting local information.* For each D dimensional point $z_i (i = 1, 2, \dots, N)$, determine a set Z_i of its k nearest neighbours including z_i , centralize Z_i as $Z_i - \bar{Z}_i e_k^T$ with \bar{Z}_i being the mean of Z_i and e_k being a column vector of all 1's, and the orthogonal basis V_i of k -dimensional tangent space consists of the d left singular vectors of the centralized matrix $Z_i - \bar{Z}_i e_k^T$ corresponding to the first d largest singular values.
- (2) *Constructing alignment matrix.* Determine the 0–1 selection matrix S_i and compute the correlation matrix W_i according to V_i . Then the alignment matrix B is constructed.
- (3) *Obtaining global coordinates.* Compute the $d+1$ smallest eigenvectors of B , then the d -dimensional global coordinates WFM ($\in R^{d \times N}$) is obtained with its elements corresponding to the 2nd to the $(d+1)$ th smallest eigenvalues. Note

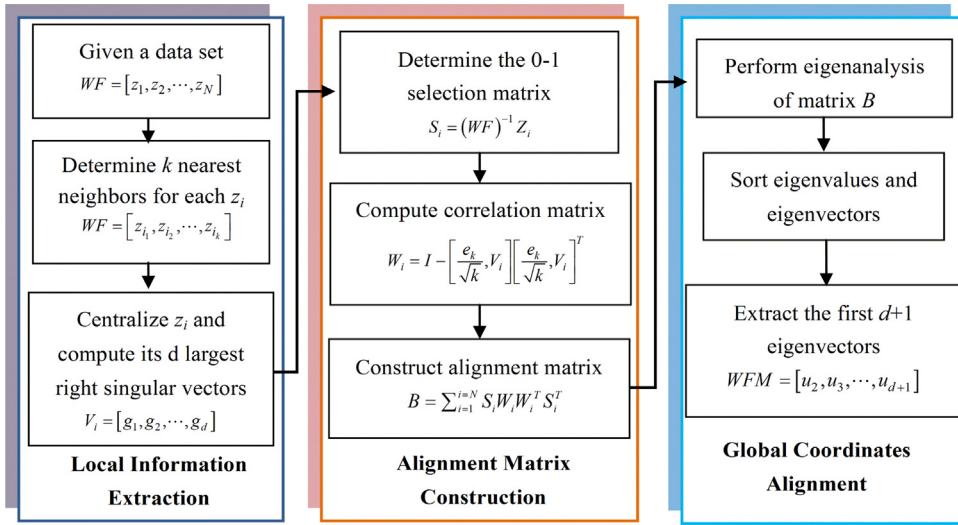


Fig. 2. The algorithm of LTSA.

the parameter d is the intrinsic dimension of the high dimensional data space, which is far less than the original dimension D .

The LTSA method has a nonlinear manifold learning ability, and is easy to implement. However, LTSA needs the adjusting of both the input parameter k for the neighbourhood identification and the intrinsic dimension d of the dataset. If the intrinsic dimension d is set larger than what it really is, much redundant information should also be preserved; if it is set smaller, useful information of the data could be left out during the dimensional reduction [33]. In our study, we found the first waveform feature manifold in the low dimensional space reveals the principal nonlinear waveform structure, and is thus taken as the extracted waveform feature in this study. Hence the dimension d is set to be 1, and the computational burden of LTSA can be reduced. The remaining parameter in the LTSA algorithm is the neighbourhood size k . As shown in Ref. [34], larger neighbourhoods will produce better conditioned eigenspaces used for extracting the global embedding for the manifold. However, with larger neighbourhoods, the accuracy of local liner approximation will suffer. In order to select an optimal k , the minimum permutation entropy criterion is used, and the extracted transient signal thereby has minimum permutation entropy.

2.3. Minimum permutation entropy criterion

There are several alternative methods for signal measurement, such as kurtosis [5], smoothness index [35], and sparsity [14]. However, the kurtosis based signal measurement method is sensitive to the outliers [35], so it is not reliable to use kurtosis as a metrics in our method. The smoothness index and sparsity are proved to be effective and reliable signal impulsiveness indicators [14,35]. However, both of them only show a larger value in the presence of fault signatures and cannot demonstrate the signal quality quantitatively. Therefore, a reliable and quantitative signal measurement method is necessary.

Bandt and Pompe presented permutation entropy (PE), a parameter of average entropy, is used to describe the complexity of time series [36]. As a statistical measuring method, the permutation entropy describes the complexity of a time series or signal measured in a physical system through phase space reconstruction, and takes into account the nonlinear behaviour of the time series [37], as often seen in vibration signals of rolling element bearings.

The value of PE can represent the randomness of the time series $\{x(i), i = 1, 2, \dots, N\}$, and it describes the local order structure of the time series. For the given time series $\{x(i), i = 1, 2, \dots, N\}$, an embedding procedure forms a vector $X_i = [x_i, x_{i+\tau}, \dots, x_{i+(m-1)\tau}]$ with the embedding dimension m , and the lag τ . Here, X_i can be arranged in an increasing order. For m different numbers, there are $m! = 1 \times 2 \times \dots \times m$ possible order patterns which are also called permutations. For a permutation π , let $f(\pi)$ denote its frequency in the time series. Then the relative frequency is $p(\pi) = f(\pi)/(N - (m-1)\tau)$. The permutation entropy for the time series is defined as follows:

$$H_p(m) = - \sum_{m=1}^{m!} p(\pi) \ln p(\pi). \quad (10)$$

The corresponding normalized entropy can be written as follows:

$$H_p = H_p(m) / \ln(m!) \quad (11)$$

If the time series is very regular, the value of H_p is close to 0. However, if the time series is random, as is in the case of white noise, the value of H_p is close to 1. A simulated signal is used to measure the PE value. Three parameters should be

Table 1
Complexity measure values of signal under various signal-to-noise ratios.

SNR	Waveform	PE value
Base signal		0.201
20dB		0.638
15 dB		0.830
10 dB		0.875
5 dB		0.964
0 dB		0.971
Write noise		0.983

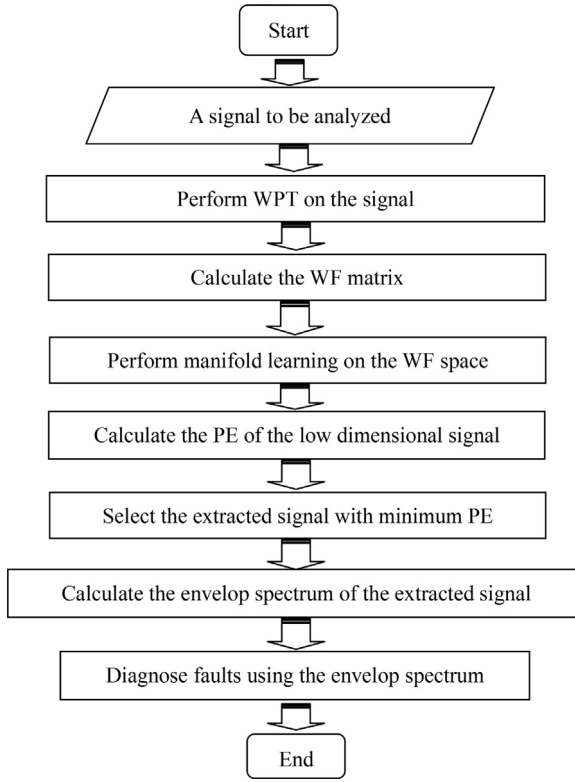


Fig. 3. The flow chart of the proposed WFM method.

selected in the permutation entropy algorithm. The data length N of the data subset taken from the original signal is set 128, the embedded dimension m is set 6 and the time delay τ is set 3 according to Ref. [37].

In Table 1, the PE values increase when the signal-to-noise ratio (SNR) decreases. Since the SNR reflects the data quality, it means that the complexity measuring method PE provides a quantitative tool to characterize the data quality of a dynamic signal. Therefore, we use minimum permutation entropy criterion to optimize the selection of parameter k for the neighbourhood identification in the manifold learning algorithm.

2.4. The algorithm of the proposed WFM method

The weak transient feature in the WF space can be captured by nonlinear manifold learning technique. Given a weak signal, the basic idea of the proposed method is illustrated in Fig. 3 and described as follows.

The proposed method is shown in Fig. 3. Before performing WPT on the signal, the mother wavelet function and the decomposition level should be properly selected. Among the wavelet families, Daubechies family (db M) is the most attractive one for wavelet analysis in mechanical signal processing, because the waveform of the daughter wavelets are

similar with the transient impulses simulated by the defect in rotating machinery. For bearing fault diagnosis, the lower order wavelets in Daubechies family, such as db2 [38], db5 [39], db10 [1,12], [40] and db12 [16] are more preferable used in discrete wavelet transform. In the proposed method, the Daubechies 10 wavelet is adopted to implement binary WPT for signal representation. To select the effective decomposition level, several methods can be adopted. Wang et al. [12] proposed the idea that the minimum bandwidth decomposed by binary WPT at maximum level needed to be three times longer than the inner race fault frequency so that sufficient bearing fault-related signatures could be retained in the desired frequency band. Shindle et al. [41] proposed a useful Shannon entropy-based criterion to obtain a best binary decomposition tree. In research [1] and [42], the maximum decomposition level is directly set 4, and is confirmed effective for vibration signal representation. In this paper, the minimum level is set 4 to ensure an informative waveform feature space, and the Shannon entropy-based best decomposition tree selection method is applied to decide the maximum level, i.e. if one node in level 4 has a Shannon entropy value greater than one, all nodes in level 4 should be further decomposed. After performing WPT on the signal, a high-dimensional wavelet feature space can be formed. In the manifold learning step, the neighbourhood sizes should be carefully selected. Since permutation entropy provides a quantitative tool for characterizing the data quality of a dynamic signal, we use minimum permutation entropy criterion to automatically select the optimal neighbourhood sizes, and the extracted transient signal in low dimensional waveform feature space thereby has minimum permutation entropy. The minimum neighbourhood size in minimum permutation entropy criterion is set 5 and the maximum size of neighbourhood is around $D/3$, where D is the dimension of the waveform feature matrix. The extracted transient signal is demodulated by envelope analysis. Finally, we use the frequency signatures of the envelope spectrum to diagnose the type of fault by identifying its characteristic frequency. The proposed WFM method is achieved by conducting the following several steps:

- Step 1:* perform binary WPT on the weak signal by Eq. (7), and the weak signal is decomposed into different time-frequency space.
- Step 2:* calculate the WF matrix by Eqs. (8) and (9) to form a high-dimensional waveform feature space.
- Step 3:* give the range of neighbourhood size for the LTSA algorithm.
- Step 4:* the low dimensional waveform feature manifold is achieved by LTSA algorithm which is described in Section 2.2. The first waveform feature manifold in the low dimensional space is selected as the extracted signal.
- Step 5:* calculate the permutation value of the extracted signal by Eqs. (10) and (11).
- Step 6:* change the neighbourhood size, repeat *steps 4 and 5*.
- Step 7:* select the extracted signal which has minimum permutation entropy.
- Step 8:* calculate the envelop spectrum and diagnose the bearing fault.

3. Simulation analysis

To verify the proposed method in extracting transient signals, a testing signal composed of white noise and periodically spaced impulses is simulated. Because the vibration signal of a defected bearing consists of periodic bursts of exponentially decaying ringing, the simulated signal can be computed by the following formula:

$$x(n) = A \sum_r e^{-\beta(n - rFs/f_m - \tau_r)/Fs} \sin(2\pi f_1 - (n - rFs/f_m - \tau_r)/Fs) \quad (12)$$

where β is the attenuation factor, equal to 500, Fs is the sampling frequency (equal to 20480 Hz), f_m is the fault characteristic frequency, set to 40 Hz, f_1 is the resonant frequency, equal to 1500 Hz, τ_r is used to simulate the randomness caused by slippage, which is subject to a discrete uniform distribution and let the initial phase ranged in $(-\pi, \pi]$. A total of 2500 samples were used for further analysis. A Gaussian white noise with a mean of 0.4 and a variance of 0.25 were added to obtain a noise-contaminated signal with a signal-to-noise ratio of -7 dB.

The simulated signal, the weak transient signal and the noise signal are shown in Fig. 4(a) and (b) respectively. Fig. 4(a) shows that the signal components consist of exponentially decaying ringing that last a short period of time. The weak transient signal and the noise signal are plotted in Fig. 4(b), the transient feature is almost swallowed by noise signal.

The proposed method is applied to analyse the noise-contaminated simulation signal. The parameters in the proposed WFM method such as the mother wavelet function, the maximum decomposition level in WPT and the range of neighbourhood size in manifold learning are selected according to the methods demonstrated in Section 2.4. A Daubechies 10 wavelet is adopted to implement binary WPT for signal representation. The decomposition levels in WPT are from level 1 to level 5. In order to conduct nonlinear manifold learning effectively, the neighbourhood size k should be carefully selected in the LTSA algorithm. Since permutation entropy can characterize data quality quantitatively, a minimum permutation entropy criterion is used to automatically select the neighbourhood size. Increasing neighbourhood size k from 5 to 35 and calculating the permutation entropy of the corresponding extracted transient signal, the optimal neighbourhood size k leading to the minimal permutation entropy relationship can be obtained. Fig. 5 shows that when the neighbourhood size is selected relatively large, the permutation entropy exhibits its minimal value at $k=26$. Therefore $k=26$ is selected as the optimal neighbourhood size.

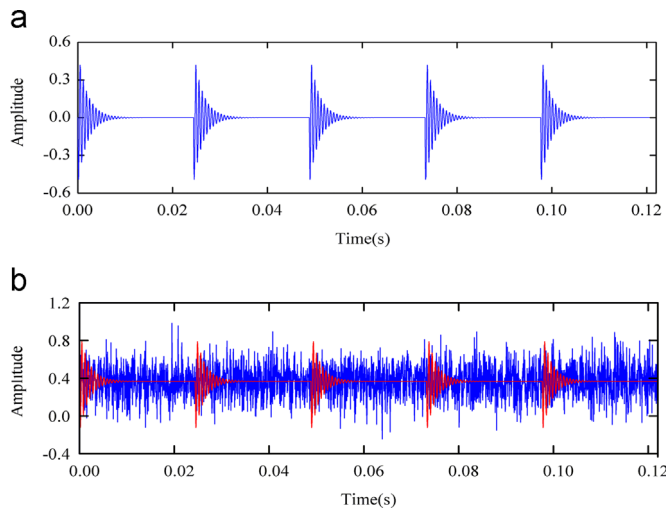


Fig. 4. (a) The periodic impulses and (b) the weak transient impulses and the noise signal.

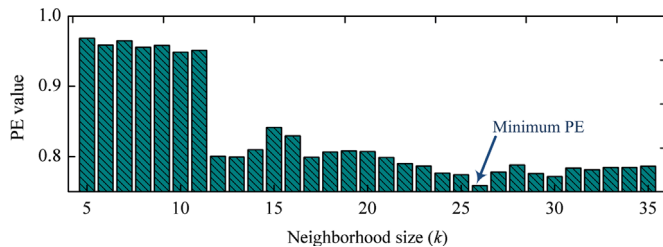


Fig. 5. The relationship between permutation entropy of the extracted signal and neighbourhood size k .

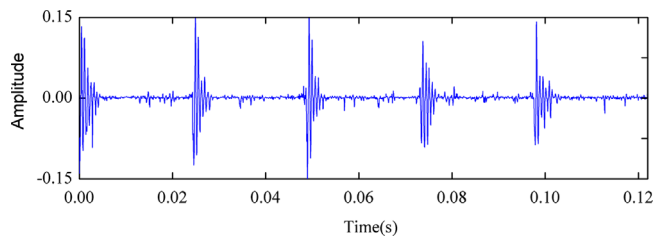


Fig. 6. The extracted transient signal by WFM.

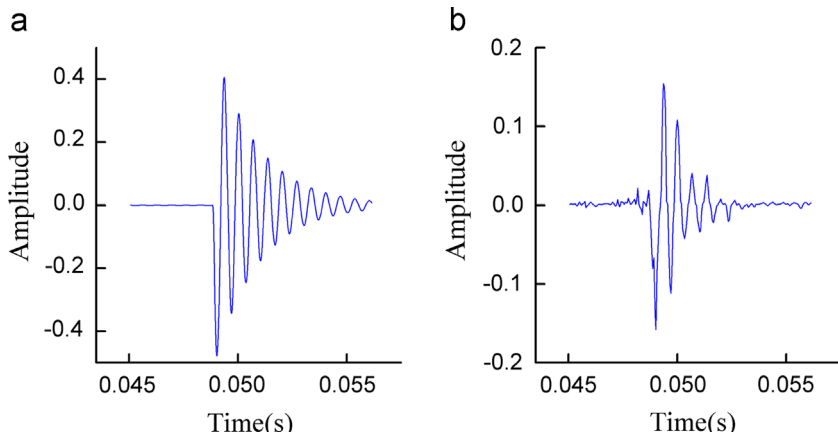


Fig. 7. (a) The simulated transient feature without noise and (b) the extracted transient feature from the weak signal by WFM.

Applying the proposed method with an optimal selected neighbourhood size to the processing of the noise contaminated signal, the extracted transient signal can be obtained as shown in Fig. 6, in which the noise is almost totally wiped off and the periodic transient feature is clearly discovered. The simulated transient feature without noise is plotted in Fig. 7(a), and

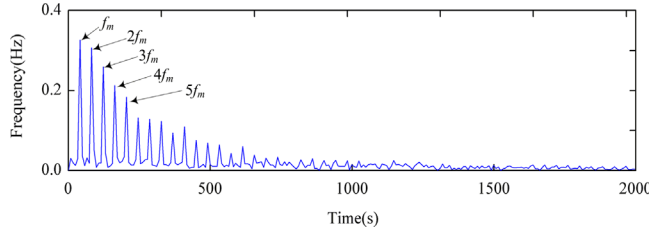


Fig. 8. The envelope spectrum of the extracted transient signal.

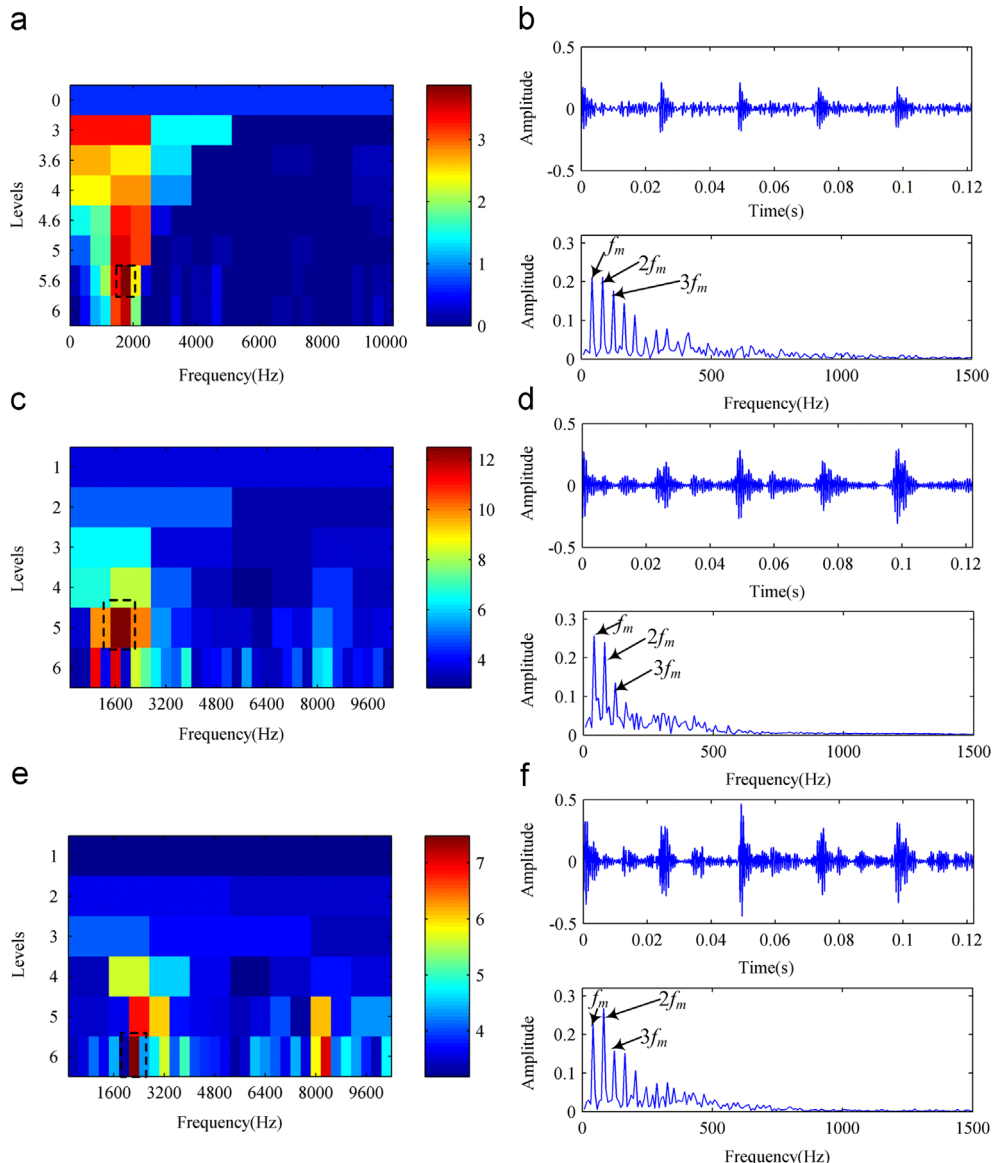


Fig. 9. The results obtained by the kurtogram-based methods. (a) The original kurtogram; (b) optimal analysis sub-band and its envelope spectrum of the original kurtogram; (c) the improved kurtogram; (d) optimal analysis sub-band and its envelope spectrum of the improved kurtogram; (e) the enhanced kurtogram; and (f) optimal analysis sub-band and its envelope spectrum of the enhanced kurtogram.

Fig. 7(b) shows the extracted transient feature by the proposed method. **Fig. 7** indicates that the WFM method successfully extracted most of the exponentially decaying ringing. Furthermore, the envelope spectrum of the extracted signal in **Fig. 8** provides a satisfied result which shows that noise is almost completely filtered out and the fault characteristic frequency f_m and a cluster of harmonics are quite effectively extracted.

For comparison purpose, the fast kurtogram, the improved kurtogram method and the enhanced kurtogram method are employed to analyse the same signal in **Fig. 4(b)**. The common points of these kurtogram-based techniques are to exploit the possibility of using the kurtosis as a measure to discover the presence of non-Gaussian components and to indicate in which frequency band the non-Gaussian components occur. Such non-Gaussian components can be considered as the structural response to an excitation, e.g. a local defect on the outer race in the case of rolling bearing faults. The paving of the original kurtogram, the improved kurtogram and the enhanced kurtogram are presented in **Fig. 9(a), (c)** and **(e)** respectively, where the node indicated by the black dash-line rectangle with maximum kurtosis value is considered to be the most useful node for providing fault signatures. The extracted transient signals from the optimal selected frequency-band by different methods and the corresponding envelope spectrum are demonstrated in **Fig. 9(b), (d)** and **(f)**. The transient signals extracted by kurtogram-based methods indicate that the selected frequency band signals with maximum kurtosis still have heavy noise and the transient features (i.e. exponentially decaying ringing) in the time domain is not very clear. Although the envelope spectrums reflect the fault characteristic frequency f_m and its harmonics of the bearing outer race, the signal-to-noise ratio is much lower than that of **Fig. 8**.

In the case of simulated bearing fault signal, it is undeniable that the proposed WFM method and the three kurtogram-based methods are effective in detecting the bearing fault characteristic frequency, which can be reflected in their envelope spectrum. However, the proposed technique is with the optimal analysing result in the sense that it extracts the periodic impulses most successfully in the time domain as shown in **Figs. 6** and **7**, whereas the periodic impulses in the filtered signals of the other three methods are less clear. Besides, in the envelop spectrum obtained by the proposed method as presented in **Fig. 8**, even the higher order harmonics (e.g., $4f_{BPFO}$, $5f_{BPFO}$, etc.) are quite evident, and the envelop spectrum obtained by the proposed method has a much higher signal-to-noise ratio. After the comparison study on the simulated signal, the result reveals that the proposed WFM method is more suitable and reliable in the detection of early stage bearing fault signals usually overwhelmed by heavy noise.

4. Experimental verification

To investigate the effectiveness of the proposed WFM method for weak signal extraction, two experimental cases are considered. They include a bearing signal with outer race defect and a bearing signal with rolling element defect.

4.1. Case 1: a bearing outer race fault signal obtained from a run-to-failure test

4.1.1. The experiment setup of the run-to-failure test

In order to reflect the real defect propagation processes, bearing run-to-failure tests were performed under normal load conditions on a specially designed test rig. The test rig is shown in **Fig. 10**. This test rig hosts four test bearings on one shaft driven by an AC motor and coupled by rub belts. The rotation speed is kept constant at 2000 rpm. A radial load of 6000 lbs. is added to the shaft and bearing by a spring mechanism. All the bearings are forced lubricated. An oil circulation system regulates the flow and the temperature of the lubricant. A magnetic plug installed in the oil feedback pipe collects the debris from the oil as an evidence of bearing degradation. The test will automatically stop when the accumulated debris adhered to the magnetic plug exceed a certain level and causes an electrical switch to close.

Four Rexnord ZA-2115 double row bearings were installed on one shaft as shown in **Fig. 10**. The bearing characteristic frequencies are usually calculated by Eqs. (13)–(17). The outer-race fault frequency f_o , the inner-race fault frequency f_i , the

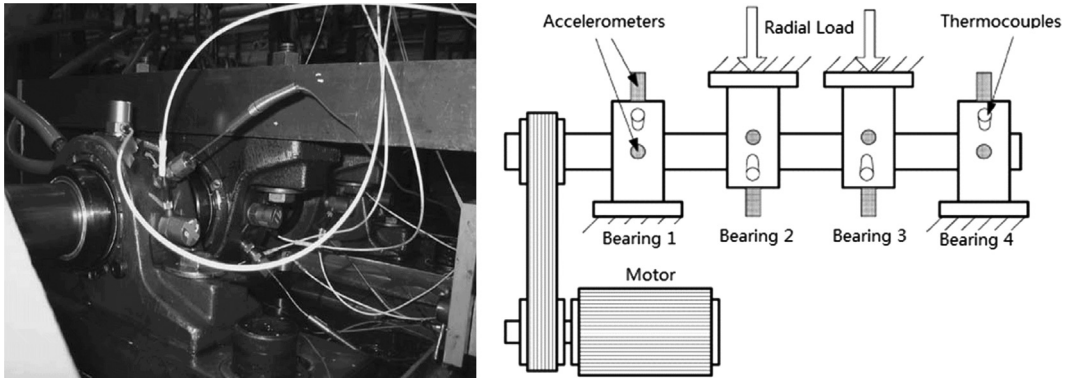


Fig. 10. Bearing test rig and sensor placement illustration.

rolling element fault frequency f_B , the fundamental cage frequency f_C and the ball spin frequency f_{BS} were formulated as follows respectively [43]:

$$f_0 = \frac{n}{2} \left(1 - \frac{d}{D_p} \cos \theta \right) f_r \quad (13)$$

$$f_I = \frac{n}{2} \left(1 + \frac{d}{D_p} \cos \theta \right) f_r \quad (14)$$

$$f_B = \frac{D_p}{d} \left[1 - \left(\frac{d}{D_p} \cos \theta \right)^2 \right] f_r \quad (15)$$

$$f_C = \frac{1}{2} \left(1 - \frac{d}{D_p} \cos \theta \right) f_r \quad (16)$$

$$f_{BS} = \frac{D_p}{2d} \left[1 - \left(\frac{d}{D_p} \cos \theta \right)^2 \right] f_r \quad (17)$$

where n is the number of balls, d is the diameter of the rolling element, D_p is the groove section size, θ is the contact angle, f_r is the shaft frequency. The structural parameters and kinematical parameters of the four experiment bearings are listed in Table 2.

A PCB 353B33 High Sensitivity Quartz ICPs Accelerometer was mounted on the housing of each bearing. For monitoring the lubrication, four thermocouples were attached to the outer race of each bearing to record bearing temperature. Vibration data of the bearings collected every 10 min by a National Instruments DAQ Card-6062E data acquisition card. The data sampling rate is 20 kHz and the data length is 20480 points. Data collection conducted by a National Instruments LabVIEW program. For more detailed information about this experiment, please refer to the literature [44], and the data can be downloaded from Prognostics Center Excellence (PCoE) through prognostic data repository contributed by Intelligent Maintenance System (IMS), University of Cincinnati [45].

4.1.2. The analysis result of the out race fault signal

The data set collected from February 12, 2004 10:32:39 to February 19, 2004 06:22:39 is used for further analysis. At the end of the test-to-failure experiment, outer race failure occurred in bearing 1. For bearing 1, the root mean square (RMS) value for the entire life cycle is shown in Fig. 11. The RMS increased to a certain level, then decreased and rose again. The fluctuating trend in Fig. 11 can be explained by the intrinsic characteristics of the damage propagating process. When the surface defect of the outer raceway just initiated, small spall or cracks were formed and later smoothed by the continuous rolling contact. When the damage spread over a wider area, the vibration level rises again.

Table 2

Structural parameters and kinematical parameters of the experiment bearing.

Bearing designation	Ball numbers	Groove section size (in.)	Contact angle	Diameter of the rolling element (in.)		
	16	0.331	15.17°	2.815		
ZA-2155 of Rexnord	f_r (Hz)	f_I (Hz)	f_0 (Hz)	f_B (Hz)	f_C (Hz)	f_{BS} (Hz)
	33	296.9	236.4	139.9	14.8	70

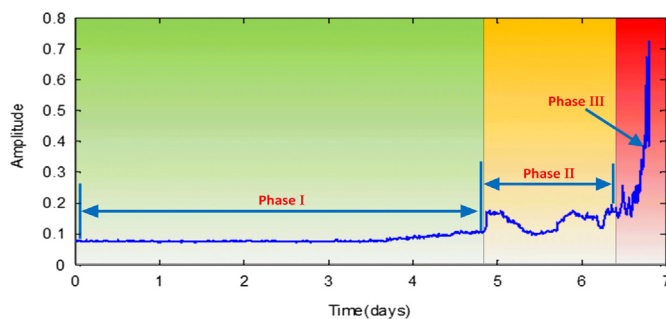


Fig. 11. The RMS of bearing 1 for the whole life cycle.

According to [6] the damage propagating process in the entire life cycle can be divided into three stages. The RMS value in the whole life cycle in Fig. 11 indicates that most of the bearing fatigue time is consumed during the period of material accumulative defect corresponding to phase I. While the period of crack propagation and development is relatively short, just as the short period between phases I and II. This means that if we use the traditional threshold-based condition monitoring approach, the response time available for the maintenance personnel to take action prior to catastrophic failure

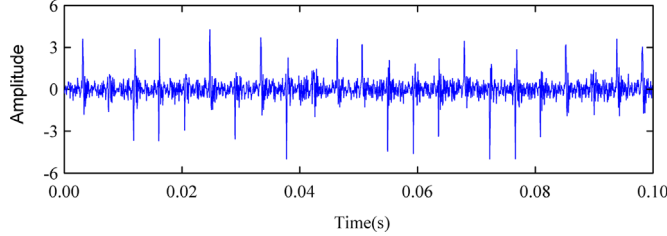


Fig. 12. The vibration signal with a serious defect.

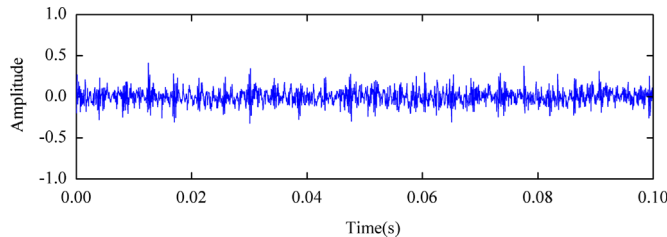


Fig. 13. The vibration signal with early stage defect.

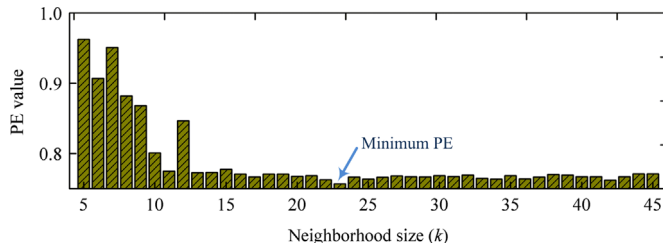


Fig. 14. The relationship of the permutation entropy value and the neighbourhood size k .

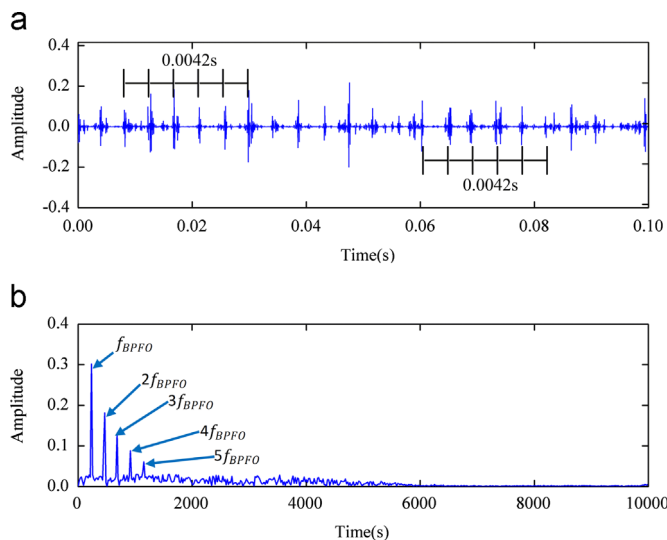


Fig. 15. The results obtained by the proposed WFM method. (a) The extracted transient signal of early stage defect by the WFM and (b) the envelope spectrum of the extracted transient signal.

after a defect is detected in the case of such bearing is very short. Therefore, it is of paramount importance to be able to accurately detect and diagnose the existence of faults occurring in the bearings at an early stage.

Fig. 12 presents the vibration signal at the last stage of the bearing test. The strong transient periodicity can be found because of the impacts produced by a serious outer race defect. After calculation, the pass frequency of outer race (f_{BPFO}) is 236.4 Hz. From the vibration signal we can easily see that the interval between the two conjoined impulses is approximately equal to $1/f_{BPFO} = 0.0042$ s, which clearly verifies the calculation.

However, when checking the historical data in phase I, about one day before the short step change as plotted in **Fig. 11**, the spall or cracks were first formed between phases I and II. The periodic impulse is very weak and the transient feature is masked by background noise as shown in **Fig. 13**.

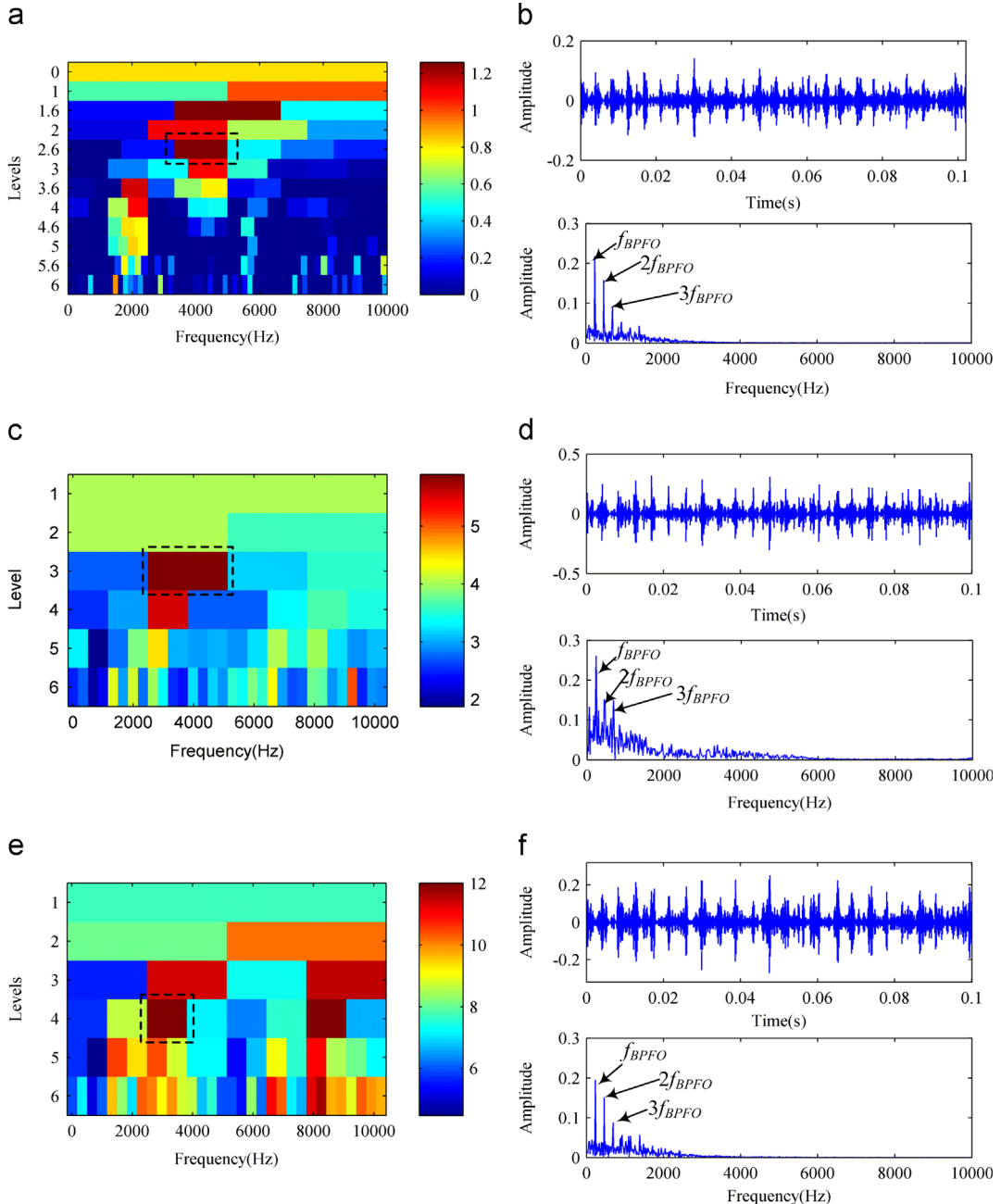


Fig. 16. The results obtained by the kurtogram-based methods. (a) The original kurtogram; (b) optimal analysis sub-band and its envelope spectrum of the original kurtogram; (c) the improved kurtogram; (d) optimal analysis sub-band and its envelope spectrum of the improved kurtogram; (e) the enhanced kurtogram; and (f) optimal analysis sub-band and its envelope spectrum of the enhanced kurtogram.

The proposed WFM method is used to enhance the weak signal. The parameters such as the mother wavelet function, the maximum decomposition level in WPT and the range of neighbourhood size in manifold learning are initially selected according to the methods demonstrated in [Section 2.4](#). At first, a Daubechies 10 wavelet also adopted to implement binary WPT for signal representation. The decomposition levels are from level 1 to level 6. Then the minimum Permutation entropy criterion is used to select the optimal neighbourhood size in the LTSA algorithm. The neighbourhood size k from 5 to 45 is scanned to find the optimal neighbourhood size that has the minimum Permutation entropy value. [Fig. 14](#) shows the Permutation entropy of the extracted transient signal corresponding to different neighbourhood sizes. As demonstrated in [Fig. 14](#), the Permutation entropy reaches its minimal value at $k = 23$. Therefore $k = 23$ is chosen as the optimal neighbourhood size.

Applying the proposed method with optimal neighbourhood for nonlinear manifold learning through minimum permutation entropy, the extracted transient signal can be obtained as shown in [Fig. 15\(a\)](#) and it reveals clearer impulses compared with the original signal demonstrated in [Fig. 13](#). The envelope analysis is performed on the extracted signal and the corresponding envelope spectrum is shown in [Fig. 15\(b\)](#). It can be seen from the envelope spectrum that noise is almost completely filtered out and the outer race fault characteristic frequency f_{BPFO} and its harmonics (e.g., $2f_{BPFO}$, $3f_{BPFO}$, $4f_{BPFO}$, $5f_{BPFO}$) are rather evident. It suggests that the defect on the outer race of the experimental bearing is effectively detected by the proposed method.

As comparison, the fast kurtogram, the improved kurtogram method and the enhanced kurtogram method are employed to analyse the same outer race fault signal shown in [Fig. 13](#). The paving of the fast kurtogram is shown in [Fig. 16\(a\)](#), where an optimal filter with a centre frequency of 4166 Hz and a bandwidth of 1667 Hz is automatically chosen. The signal filtered by the optimal filter and the envelope spectrum of the filtered signal shows the fault related signatures in [Fig. 16\(b\)](#). The improved kurtogram is used to analyse the same outer race fault signal. The paving of the improved kurtogram is plotted in [Fig. 16\(c\)](#), in which the node (3, 1) is the most valuable node for providing outer race fault signatures. The envelope spectrum of the signal extracted from node (3, 1) by WPT provides information about inner race faults in [Fig. 16\(d\)](#). The enhanced kurtogram is also adopted to process the weak signal and the corresponding paving is shown in [Fig. 16\(e\)](#). The node (4, 2) is selected for further analysis. The filtered signal and its envelope spectrum are plotted in [Fig. 16\(f\)](#). The extracted transient signals from the optimal selected frequency band by different methods and the corresponding envelope spectrum are shown in [Fig. 16\(b\), \(d\) and \(f\)](#) respectively. By visual inspection, the transient signals extracted by kurtogram-based methods still have heavy noise. Besides, although the envelope spectrum reflects the fault frequency and its harmonics, the signal-to-noise ratio is much lower than that of [Fig. 15\(b\)](#).

In the case of bearing outer race fault diagnosis, the result indicates that both of the proposed WFM method and the kurtogram-based methods are effective in incipient outer race defect detection. However, the result obtained by the proposed method presented in [Fig. 15\(a\)](#) reveals clearer impulses compared with the signal extracted by the kurtogram-based methods shown in [Fig. 16](#). Besides, in the envelop spectrum obtained by the proposed method presented in [Fig. 15\(b\)](#), even the higher order harmonics (e.g., $4f_{BPFO}$, $5f_{BPFO}$) are evident, and the signal-to-noise ratio of the envelope spectrum plotted in [Fig. 15\(b\)](#) is much higher than that shown in [Fig. 16](#). It means that the proposed WFM method is able to more clearly extract the bearing fault characteristics than the kurtogram-based methods.

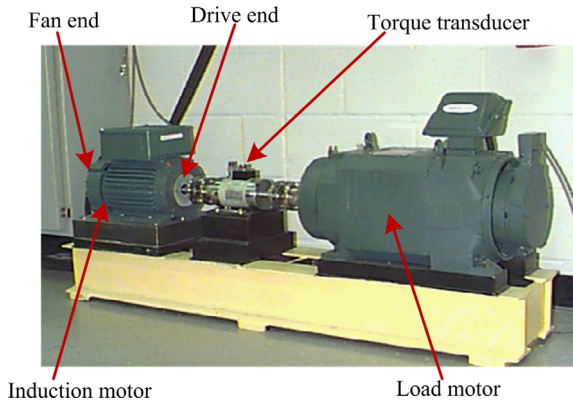


Fig. 17. The bearing test rig.

Table 3

The structural parameters of the tested bearing.

D_I (in.)	D_O (in.)	T_H (in.)	D_B (in.)	D_P (in.)	N
0.9843	2.0472	0.5906	0.3126	1.537	9

D_I is the inside diameter, D_O is the outside diameter, T_H is the thickness, D_B is the ball diameter, D_P is the pitch diameter, N is the number of rolling elements.

4.2. Case 2: a bearing rolling element fault signal obtained from an experiment motor

4.2.1. The experiment setup of the bearing defect test

A bearing signal with slight rolling element defect is used to further verify the WFM method in extracting the periodic transient impulses. The bearing data are obtained from the Case Western Reserve University (CWRU) Bearing Data Centre Website [46]. The data set was acquired by using an experimental setup shown in Fig. 17. The test rig consists of a 2-horse power motor, a torque transducer, a dynamometer, and control electronics (not shown).

Table 4

Information of the tested bearing with rolling element defect.

Defect location	$D_S (D \times W)$ (in.)	R (RPM)	f_C (Hz)	f_B (Hz)	f_{BS} (Hz)	f_I (Hz)	f_o (Hz)
Rolling element	0.011×0.007	1732	11	115	57	142	88

D_S is the defect size, R is the rotating speed, f_C is the fundamental cage frequency, f_B is the rolling element fault frequency, f_{BS} is the ball spin frequency, f_I is the inner-race fault frequency, and f_o is the outer-race fault frequency.

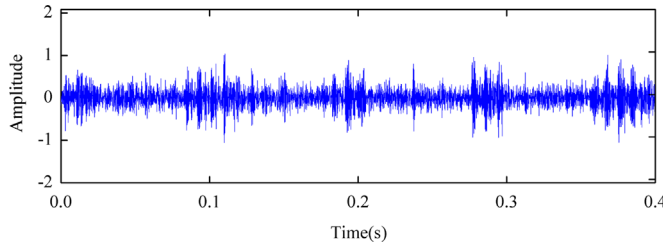


Fig. 18. The original noise corrupted rolling element fault signal.

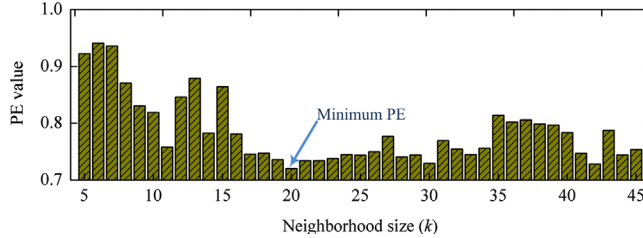


Fig. 19. The relationship of the permutation entropy value and the neighbourhood size k .

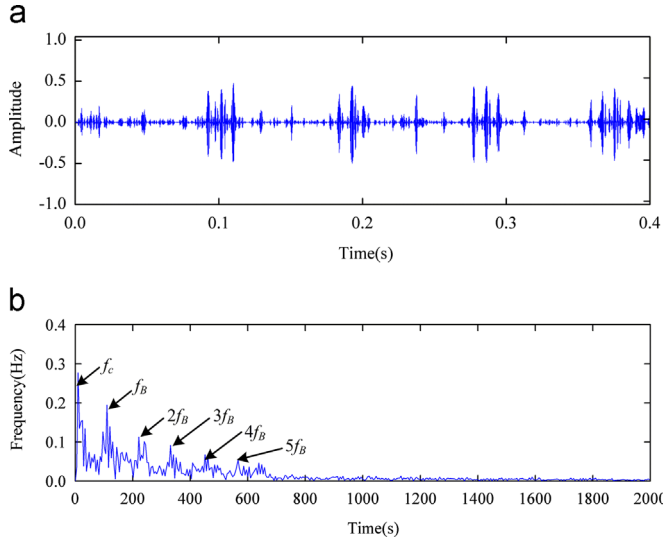


Fig. 20. The result obtained by WFM method. (a) the extracted transient impulses by the WFM method, (b) the envelope spectrum of the extracted signal.

The test bearings support the motor shaft. Vibration data were collected using accelerometers, attached to the housing with magnetic bases. The sampling frequency was set to 12 kHz for fan end bearing experiments. The bearings used in this test are the deep groove ball bearings 6205-2RS JEM SKF. The details of the geometry of this type of bearing are given in **Table 3**. Single point defect was seeded on the rolling element using electro-discharge machining (EDM). The signal with rolling element defect is chosen for the following analysis. The defect-related parameters, including the defect size, the rotating speed and the calculated characteristic frequency according to Eqs. (13)–(17), of the selected signal are provided in **Table 4**.

4.2.2. The transient impulse extraction result of the rolling element fault signal

The original noise contaminated signal with a slight rolling element defect is displayed in **Fig. 18**, the transient impulses are seriously corrupted by the background noise. In order to accurately locate the fault position, the clean transient impulses should be effectively extracted.

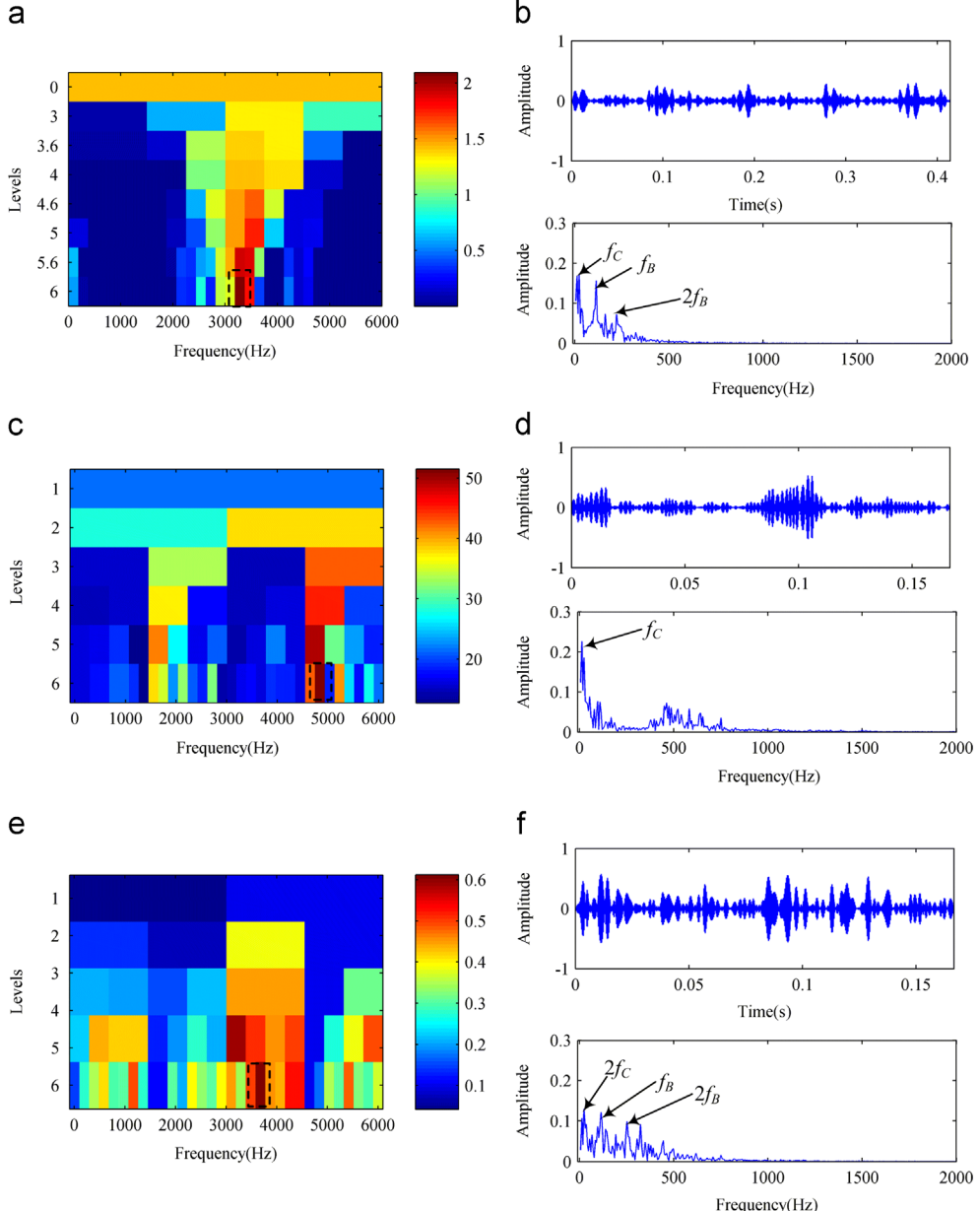


Fig. 21. The results obtained by the kurtogram-based methods. (a) The original kurtogram; (b) optimal analysis sub-band and its envelope spectrum of the original kurtogram; (c) the improved kurtogram; (d) optimal analysis sub-band and its envelope spectrum of the improved kurtogram; (e) the enhanced kurtogram; and (f) optimal analysis sub-band and its envelope spectrum of the enhanced kurtogram.

The proposed WFM method is employed to extract the transient impulses from the weak rolling element fault signal. According to the methods shown in [Section 2.4](#), the parameters in the WFM algorithm such as the mother wavelet function, the maximum decomposition level in WPT and the range of neighbourhood size in manifold learning are initially selected as follows. The dB 10 is selected as the mother wavelet, the decomposition levels are from level 1 to 6. The relationship between the permutation entropy and the neighbourhood size is plotted in [Fig. 19](#). The optimal neighbourhood size in the LTSA algorithm is set to 20 according to the minimum permutation entropy criterion.

Then the transient impulses can be obtained from the original weak signal by the WFM method. [Fig. 20\(a\)](#) demonstrates the extracted signal, it can be visually inspected that the weak transient impulses are effectively uncovered by the proposed method and the noise components are almost totally cleared out. The envelope spectrum of the extracted signal is presented in [Fig. 20\(b\)](#), the fundamental cage frequency f_C , the rolling element fault frequency f_B and its harmonics are very evident.

In order to investigate the improved performance of the proposed method in weak rolling element fault signature extraction, the fast kurtogram, the improved kurtogram method and the enhanced kurtogram method are used to analysis the same rolling element fault signal, as shown in [Fig. 18](#). The paving of the fast kurtogram is presented in [Fig. 21\(a\)](#), where an optimal filter with a centre frequency of 3281 Hz and a bandwidth of 187 Hz. The signal filtered by the optimal selected frequency band and the envelope spectrum of the filtered signal are demonstrated in [Fig. 21\(b\)](#), in which the fundamental cage frequency and the rolling element fault frequency are evident. The improved kurtogram is utilized to process the same rolling element fault signal. The paving of the improved kurtogram is shown in [Fig. 21\(c\)](#), in which the node (6, 25) is considered as the most valuable node for providing rolling element fault signatures. However, the envelope spectrum of the extracted signal just provides the information about fundamental cage frequency as shown in [Fig. 21\(d\)](#). The enhanced kurtogram is also employed to analyse the weak signal and the corresponding paving is shown in [Fig. 21\(e\)](#). The node (6, 19) is selected for further analysis. The extracted signal and its envelope spectrum are plotted in [Fig. 21\(f\)](#), in which the second order of the fundamental cage frequency and the rolling element fault frequency are apparent.

In the case of weak rolling element fault signature detection, it is undeniable that the kurtogram-based methods have an ability to extract the rolling element fault signatures to some extent. However, by visual inspection, the transient signals extracted by kurtogram-based methods are still corrupted by noise. Besides, the fault frequency and its harmonics in the envelope spectrum are less clear, when compared with the envelope spectrum obtained by the proposed method as shown in [Fig. 20\(b\)](#).

In [Section 4](#), two real bearing fault signals are analysed by the proposed WFM method, the fast kurtogram method, the improved kurtogram method and the enhanced kurtogram method. Case 1 concerns the real bearing outer-race fault signal acquired from a run-to-failure experiment. Case 2 concerns the rolling element fault signal with artificial defect seeded by EDM. As a result, after the comprehensive comparisons have been done, the proposed WFM method shows best performance for bearing fault diagnosis in the two cases studies. The experimental results verified the effectiveness of the proposed WFM method in bearing incipient defect detection and providing potential proof to the maintenance personnel for diagnosis decision-making.

5. Conclusions

Aiming at the shortcomings of the kurtogram-based methods, this paper presents a WFM method to extract the transient signals through performing nonlinear manifold learning on the waveform feature space obtained by binary WPT. In the simulation analysis and experimental verification, both of the proposed method and the kurtogram-based methods have the ability to extract the bearing fault signatures. However, the results obtained by the proposed method have better waveform characteristics. Besides, the signal-to-noise ratio of the envelope spectrum obtained by WFM is much higher than the kurtogram-based methods. The comparative studies on the simulated and real bearing fault signals indicate that the proposed WFM method outperforms the kurtogram-based methods. The results validate the proposed method is able to extract fault signatures from weak signals and can be regarded as an effective and reliable method for rolling element bearing faults diagnosis at an early stage.

Acknowledgement

This research is supported by the Shaanxi Overall Innovation Project of Science and Technology (No. 2013KTCQ01-06). Special thanks should be expressed to the editors and anonymous reviewers for their valuable suggestions.

References

- [1] Y.G. Lei, J. Lin, Z.J. He, et al., Application of an improved kurtogram method for fault diagnosis of rolling element bearings, *Mech. Syst. Signal Process.* 25 (2011) 1738–1749.
- [2] Y.G. Lei, Z.J. He, Y.Y. Zi, Fault diagnosis of rotating machinery based on multiple ANFIS combination with gas, *Mech. Syst. Signal Process.* 21 (2007) 2280–2294.
- [3] C. Hory, N. Martin, A. Chehikian, Spectrogram segmentation by means of statistical features for non-stationary signal interpretation, *Signal Process. IEEE Trans.* 12 (2002) 2915–2925.

- [4] L. Angrisani, P. Daponte, M. D'Apuzzo, A method for the automatic detection and measurement of transients. Part I: the measurement method, *Measurement* 25 (1999) 19–30.
- [5] J. Antoni, R.B. Randall, A stochastic model for simulation and diagnostics of rolling element bearings with localized faults, *Journal of Vibration and Acoustics*, vol. 125 (3), pp. 282–289.
- [6] H. Qiu, J. Lee, J. Lin, G. Yu, Wavelet filter-based weak signature detection method and its application on roller bearing prognostics, *J. Sound Vib.* 289 (2006) 1066–1090.
- [7] R.B. Randall, Frequency Analysis (Bruel&Kjaer), 1987, 344.
- [8] L. Cohen, Time-Frequency Analysis: Theories and Applications, Prentice-Hall, Englewood Cliffs, NJ, 1995.
- [9] S. Mallat, A Wavelet Tour of Signal Processing, Academic Press, New York, 1999.
- [10] Z.J. He, Y.Y. Zi, Q.F. Meng, Fault Diagnosis Principle of Non-stationary Signal and Applications to Mechanical Equipment, Higher Education Press, Beijing, 2001 (in Chinese).
- [11] J. Antoni, Fast computation of the kurtogram for the detection of transient faults, *Mech. Syst. Signal Process.* 21 (2007) 108–124.
- [12] D. Wang, P.W. Tse, K.L. Tsui, An enhanced Kurtogram method for fault diagnosis of rolling element bearings, *Mech. Syst. Signal Process.* 35 (2013) 176–199.
- [13] T. Barszcz, A. Jablonski, A novel method for the optimal band selection for vibration signal demodulation and comparison with the kurtogram, *Mech. Syst. Signal Process.* 25 (2011) 431–451.
- [14] P.W. Tse, D. Wang, The design of a new sparsogram for fast bearing fault diagnosis: Part 1 of the two related manuscripts that have a joint title as two automatic vibration-based fault diagnostic methods using the novel sparsity measurement – Parts 1 and 2, *Mech. Syst. Signal Process.* 40 (2013) 520–544.
- [15] Y. Wang, M. Liang, Identification of multiple transient faults based on the adaptive spectral kurtosis method, *J. Sound Vib.* 331 (2012) 470–486.
- [16] N.G. Nikolaou, I.A. Antoniadis, Rolling element bearing fault diagnosis using wavelet packets, *NDT & E Int.* 35 (2002) 197–205.
- [17] S.T. Rowewi, L.K. Saul, Nonlinear dimensionality reduction by locally linear embedding, *Science* 290 (2000) 2323–2326.
- [18] J.B. Tenenbaum, V. Silva, J.C. Langford, A global geometric framework for nonlinear dimensionality reduction, *Science* 290 (2000) 2319–2323.
- [19] Z. Zhang, H. Zha, Principal manifolds and nonlinear dimensionality reduction via tangent space alignment, *J. Scientific Comput.* 26 (2005) 313–338.
- [20] M. Belkin, P. Niyogi, Laplacian eigenmaps for dimensionality reduction and data representation, *Neural Comput.* 15 (2003) 1373–1396.
- [21] M. Li, J. Xu, J. Yang, et al., Multiple manifolds analysis and its application to fault diagnosis, *Mech. Syst. Signal Process.* 23 (2009) 2500–2509.
- [22] Q. Jiang, M. Jia, J. Hu, et al., Machinery fault diagnosis using supervised manifold learning, *Mech. Syst. Signal Process.* 23 (2009) 2301–2311.
- [23] I. Lopez, N. Sarigul-Klijn, Distance similarity matrix using ensemble of dimensional data reduction techniques: vibration and aerocoustic case studies, *Mech. Syst. Signal Process.* 23 (2009) 2287–2300.
- [24] Q. He, Vibration signal classification by wavelet packet energy flow manifold learning, *J. Sound Vib.* 332 (2012) 1881–1894.
- [25] L. Jiang, J. Xuan, T. Shi, Feature extraction based on semi-supervised kernel marginal Fisher analysis and its application in bearing fault diagnosis, *Mech. Syst. Signal Process.* 41 (2013) 113–126.
- [26] Z. Su, B. Tang, J. Ma, et al., Fault diagnosis method based on incremental enhanced supervised locally linear embedding and adaptive nearest neighbour classifier, *Measurement* 48 (2014) 136–148.
- [27] B. Tang, T. Song, F. Li, et al., Fault diagnosis for a wind turbine transmission system based on manifold learning and Shannon wavelet support vector machine, *Renew. Energy* 62 (2014) 1–9.
- [28] Y. Huang, X.F. Zha, J. Lee, et al., Discriminant diffusion maps analysis: a robust manifold learner for dimensionality reduction and its applications in machine condition monitoring and fault diagnosis, *Mech. Syst. Signal Process.* 34 (2013) 277–297.
- [29] Z. Li, X. Yan, Z. Tian, et al., Blind vibration component separation and nonlinear feature extraction applied to the nonstationary vibration signals for the gearbox multi-fault diagnosis, *Measurement* 46 (2013) 259–271.
- [30] Q. He, X. Wang, Time-frequency manifold correlation matching for periodic fault identification in rotating machines, *J. Sound Vib.* 332 (2013) 2611–2626.
- [31] J. Wang, Q. He, F. Kong, Automatic fault diagnosis of rotating machines by time-scale manifold ridge analysis, *Mech. Syst. Signal Process.* 40 (2013) 237–256.
- [32] Q. He, Time-frequency manifold for nonlinear feature extraction in machinery fault diagnosis, *Mech. Syst. Signal Process.* 35 (2013) 200–218.
- [33] M.Y. Fan, H. Qiao, B. Zhang, Intrinsic dimension estimation of manifolds by incising balls, *Pattern Recognit.* 42 (2009) 780–787.
- [34] H. Zha, Z. Zhang, Spectral properties of the alignment matrices in manifold learning, *SIAM Rev.* 51 (2009) 545–566.
- [35] I.S. Bozchalooi, M. Liang, A smoothness index-guided approach to wavelet parameter selection in signal de-noising and fault detection, *J. Sound Vib.* 308 (2007) 246–267.
- [36] C. Bandt, B. Pompe, Permutation entropy: a natural complexity measure for time series, *Phys. Rev. Lett.* 88 (2002) 174102-1–174102-4.
- [37] R.Q. Yan, Y.B. Liu, R.X. Gao, Permutation entropy: a nonlinear statistical measure for status characterization of rotary machines, *Mech. Syst. Signal Process.* 29 (2012) 474–484.
- [38] X. Lou, K.A. Loparo, Bearing fault diagnosis based on wavelet transform and fuzzy inference, *Mech. Syst. Signal Process.* 18 (2004) 1077–1095.
- [39] C. Wang, R.X. Gao, Wavelet transform with spectral post-processing for enhanced feature extraction, *Instrum. Meas. IEEE Trans.* 52 (2003) 1296–1301.
- [40] B. Liu, Selection of wavelet packet basis for rotating machinery fault diagnosis, *J. Sound Vib.* 284 (2005) 567–582.
- [41] A. Shinde, Z. Hou, A wavelet packet based sifting process and its application for structural health monitoring, *Struct. Health Monit.* 4 (2005) 153–170.
- [42] E.Y. Kim, Y.J. Lee, S.K. Lee, Heath monitoring of a glass transfer robot in the mass production line of liquid crystal display using abnormal operating sounds based on wavelet packet transform and artificial neural network, *J. Sound Vib.* 331 (2012) 3412–3427.
- [43] R.B. Randall, J. Antoni, Rolling element bearing diagnostics—a tutorial, *Mech. Syst. Signal Process.* 25 (2011) 485–520.
- [44] H. Qiu, J. Lee, J. Lin, et al., Robust performance degradation assessment methods for enhanced rolling element bearing prognostics, *Adv. Eng. Inform.* 17 (2003) 127–140.
- [45] J. Lee, H. Qiu, G. Yu, et al., Rexnord Technical Services: Bearing Data Set, Moffett Field, CA: IMS, Univ. Cincinnati. NASA Ames Prognostics Data Repository, NASA Ames, 2007.
- [46] (<http://www.eecs.case.edu/laboratory/bearing>) (accessed 01.04.11).